Physical Optics and Electronics

Academic Research Staff

Professor Rajeev J. Ram, Dr. Holger Schmidt, Elizabeth Bruce

Graduate Students

Mathew C. Abraham, Song-Ho Cho, George Cragg, Harry L. T. Lee, Tom Liptay, Peter Mayer, Kevin p. Pipe, Farhan Rana, Margaret Wang

Undergraduate Students

Brian Goldberg

Introduction

The Physical Optics and Electronics Group within the Research Laboratory of Electronics addresses science questions that arise during the development and application of new devices. While the central research thrust is on optoelectronic devices the group's efforts have branched into electron hydrodynamics, quantum transport and micromagnetics. This report details the research milestones listed below:

Accurate models for noise in various semiconductor lasers have been developed and tested. The devices studied include
- Surface emitting lasers
- Quantum cascade lasers
- Mode-locked semiconductor lasers

Heterojunction thermoelectric cooling was investigated in bipolar devices. The first models for Seebeck and Peltier coefficients in a bipolar device were developed. In addition a test station for microthermal measurements was fabricated and used to study the thermal performance of InP, GaAs and GaSb lasers.

A low temperature (4K) scanning probe microscope facility has been established. This single microscope has been used for scanning tunneling, contact atomic force microscopy and non-contact atomic force-microscopy.

Quantum Theory of Noise and Timing Jitter in Mode-Locked Laser

Sponsor

DARPA-PACT

Research Staff

Farhan Rana, Professor Rajeev J. Ram

Short pulse generation from mode-locked lasers has important applications in electro-optic sampling, optical analog-to-digital conversion, optical communication systems, and ultra-fast optical measurements [1]. Low noise performance of mode-locked lasers is critical to most of these applications. We have extended the previous work [2-4] on the noise of optical pulses in mode-locked lasers to actively and hybrid mode-locked lasers with phase modulation and dispersion. Our results have important applications in realizing semiconductor mode-locked lasers with low timing jitter since in semiconductor mode-locked lasers amplitude modulation is always accompanied by phase modulation as a result of the carrier density dependent refractive index.

The linear operator [2] that describes the slow time evolution of the pulse fluctuations in a mode-locked laser is in most cases not Hermitian (i.e. not self-adjoint). This operator can be non-Hermitian in the presence of a number of different factors including, for example, group velocity dispersion, active phase modulation, and self-phase modulation accompanying dynamic gain/loss saturation (when the refractive index of the gain/loss medium is carrier density dependent). In these cases the steady state optical pulse is generally complex and chirped. The eigen-modes of the non-Hermitian operator describing the time evolution of the pulse fluctuations are not mutually orthogonal. Pulse fluctuations are usually studied by expanding the solution in the presence of noise in terms of the eigen-modes of this operator [2-5]. We show that the non-orthogonality of the eigen-modes can result in excess quantum noise in the pulse photon number, phase, frequency, and timing fluctuations. The situation is somewhat analogous to that in gain-guided laser amplifiers and non-Hermitian laser oscillators, where the excess spontaneous emission noise is described by the Petermann's factor [6-9]. Previously reported work on the noise in mode-locked lasers has either not considered non-Hermitian cases [2,3], or assumed from the outset specific conditions which allowed only real unchirped steady state pulses that do not exhibit excess noise [4,5].

We have developed a fully self-consistent quantum mechanical model for the noise in optical pulses in both linear and non-linear (including dynamic gain/loss saturation) mode-locked laser systems that are characterized by a non-Hermitian pulse evolution operator. Our results indicate that the excess noise factor can be quite large. In semiconductor mode-locked lasers this factor can exceed 10 for the mean square timing and frequency noise (Fig. 1). In non-Hermitian mode-locked laser systems the pulse photon number, phase, timing and frequency fluctuation operators have first order contributions from the noise in the eigen-modes of all order. In Hermitian mode-locked systems to first order only the first two eigen-modes contribute to these fluctuation operators [2,3]. The contribution to the pulse noise from the higher order eigen-modes renormalizes the low frequency fluctuations. This renormalization partially compensates for the excess noise.

For linear (and mildly non-linear) mode-locked laser systems the chirp (β) of the steady state pulse is a good measure of the degree of non-orthogonality of the eigen-modes. When the magnitude of the pulse chirp exceeds a critical critical value (β=0.577) the perturbative expansion for the pulse fluctuations diverges exponentially as more eigen-modes are included in the expansion (Fig. 3). In most semiconductor mode-locked lasers the pulse chirp far exceeds this critical value beyond which the perturbative expansion fails to converge. The actual pulse

remains stable. We have developed a renormalized perturbation theory that always converges and gives accurate answers for the noise in the pulse (Fig. 3). The large noise usually observed in semiconductor mode-locked lasers [11], compared to fiber lasers [12], is thought to be mainly due to the incomplete inversion of the gain medium in semiconductor lasers. Our results show that the excess noise coming from the non-orthogonality of the eigen-modes is a much larger effect.

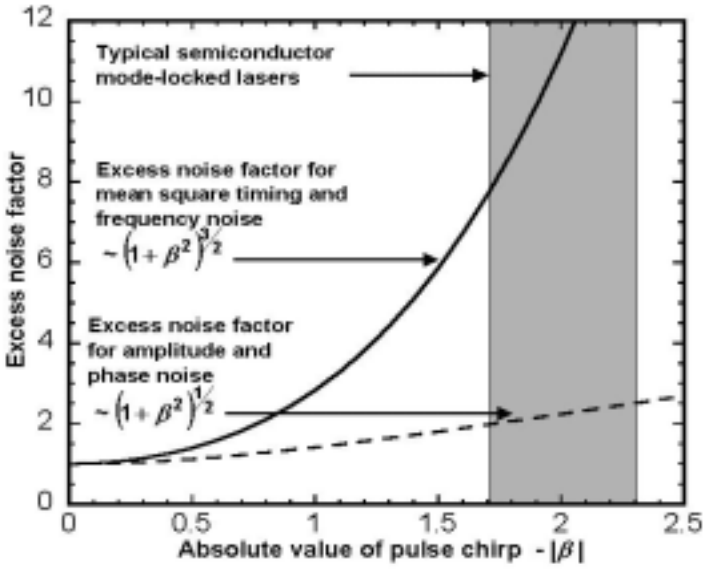

Fig. 1: Excess noise factor as a function of the magnitude of the pulse chirp (β) for an actively mode-locked laser in the presence of active phase modulation, group velocity dispersion, and non-linear self-phase modulation arising from dynamic gain saturation. The shaded region represents the chirp in typical semicondctor mode-locked lasers [11]. The phase modulation index is related to the amplitude modulation index by the semiconductor α-parameter, which is assumed to be equal to 3.0.

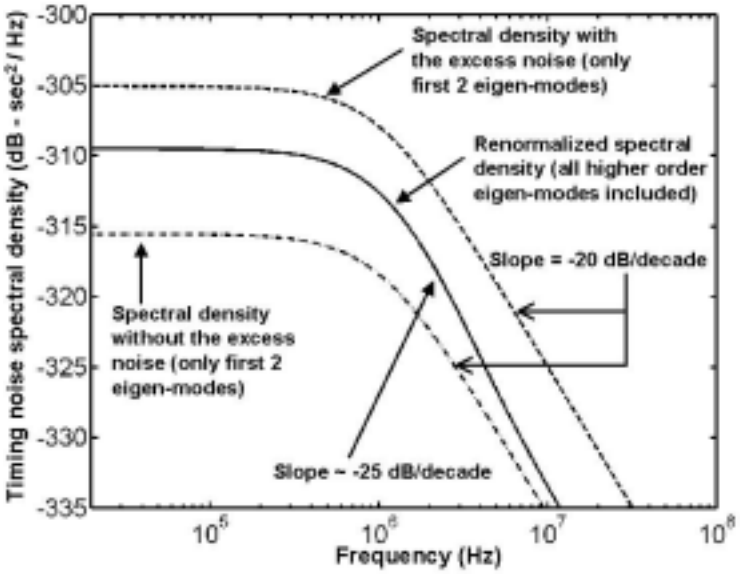

Fig. 2: Spectral density of the timing jitter for a 2.0 GHz, 1.55 μm actively mode-locked semiconductor laser in the presence of active phase modulation, group velocity dispersion, and non-linear self-phase modulation. The chirp in the steady state pulse is $=\beta=-2.0$. The dash-dotted represents the case when the excess noise is ignored and only the first two eigen-modes are used in the perturbative expansion. The dashed line is the case when only the first two eigen-modes are inlcuded and the excess noise factor is also taken into account. The solid line is the complete solution obtained when the excess noise and all the higher order eigen-modes are taken into account. The higher order eigen-modes not only renormalize the low frequency timing noise spectrum but also change the slope of the decay beyond the roll-off point.

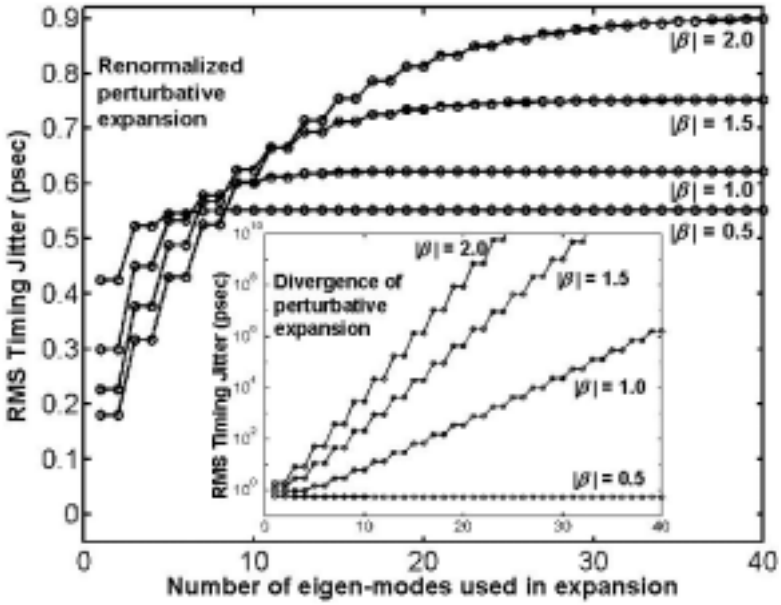

Fig. 3: Root mean square (RMS) timing jitter for a 1.0 GHz, 1.55 μm actively mode-locked semiconductor laser in the presence of active phase modulation, group velocity dispersion, and non-linear self-phase modulation. The curves are plotted as a function of the number of eigen-modes used in the perturbative expansion for different absolute values of the chirp (β) in the steady state pulse. The conventional perturbative expansion (shown in the inset) fails to converge and diverges exponentially when the pulse chirp exceeds the critical value of ~0.577. The renormalized perturbative expansion converges for all values of the pulse chirp.

References

1. P. W. Juodawlkis, J. C. Twichell, G. E. Betts, J. J. Hargreaves, R. D. Younger, J. L. Wasserman, F. J. O'Donnell, K. G. Ray, R. C. Williamson, “Optically sampled analog-to-digital converters,” Trans. Mirowave Theory and Tech. **49**, 1840-1853 (2001).
2. H. A. Haus, “A theory of forced mode-locking,” J. Quantum Electronics **11**, 323-330 (1975).
3. D. R. Hjelme, A. R. Mickelson, “Theory of timing jitter in actively mode-locked lasers,” IEEE J. Quantum Electronics, **28,** 1594-1606 (1992).
4. H. A. Haus, A. Mecozzi, “Noise of mode-locked lasers,” IEEE J. Quantum Electronics, **29,** 983-996 (1993). H. A. Haus, M. Margalit, C. X. Yu, “Quantum noise of a mode-locked laser,” J. Opt. Soc. Am. B **17**, 1240-1256 (2000).
5. L. A. Jiang, M. E. Grein, H. A. Haus, E. P. Ippen, “Noise of Mode-locked semiconductor lasers,” J. Select. Quantum Electronics **7**, 159-167 (2001).
6. K. Petermann, “Calculated spontaneous emission factor for double-heterostructure injection lasers with gain-induced waveguiding,” J. Quantum Electronics 15, 566-570 (1979).
7. H. A. Haus, S. Kawakami, “On the excess spontaneous emission factor in gain-guided laser amplifiers,” J. Quantum Electronics 21, 63-69 (1985).
8. A. E. Siegman, “Excess spontaneous emission in non-Hermitian optical systems. I. Laser amplifiers,” Phys. Rev. A 39, 1253-1263 (1989).
9. A. E. Siegman, “ Excess spontaneous emission in non-Hermitian optical systems. II. Laser oscillators,” Phys. Rev. A 39, 1264-1268 (1989).
10. D. Von Der Linde, “Characterization of the noise in continuously operating mode-locked lasers,'' J. Appl. Phys. B **39**, 201-217 (1986).
11. D. J. Derickson, P. A. Morton, J. E. Bowers, “Comparison of timing jitter in external and monolithic mode-locked semiconductor lasers,” Appl. Phs. Lett., **59,** 3372-3374 (1991).
12. T. R. Clark, T. F. Carruthers, P. J. Mathews, I. N. Duling III, “Phase noise measurements of ultrastable 10 GHz harmonically modelocked fibre laser,'' Elec. Lett. **35**, 720-721 (1999).

Current Noise in Semiconductor Lasers

Sponsor

DARPA-RLICS, ONR

Research Staff

Farhan Rana, Peter Mayer, Professor Rajeev J. Ram

Accurate modeling of the current noise in semiconductor lasers is desired for many different applications. It is well known that high impedance suppression of the current noise in semiconductor lasers leads to photon number squeezing in the laser output [1,2]. However, the magnitude of the current noise is not well known and, therefore, it is difficult to predict the limits on the amount of squeezing achievable in semiconductor lasers. Accurate modeling of the current noise is also important in semiconductor cascade laser structures in which PN junctions are connected electrically in series [5-8]. In such devices the degree of correlation in photon emission events in different junctions depends on the magnitude of the current noise. Current noise is related to the fast electron-photon dynamics inside the active region of the laser, and can therefore be used as a non-optical tool to study these dynamics.

Many laser noise models that have appeared in the literature simply assume statistics for the current noise from the beginning and feed these into the standard laser noise models to calculate the photon noise [5,9]. Such an approach is not self-consistent since a significant portion of the

current noise is in fact a circuit response to the carrier density fluctuations inside the active region. In references [1,2] self-consistent models of the current noise in semiconductor lasers have been presented. These models assume from the start a fixed relation between the carrier density fluctuations inside the active region and the fluctuations in the potential difference across the active region. This assumption, although valid for homo-junction semiconductor lasers, does not hold for hetero-junction lasers. All the current noise models also ignore the carrier density fluctuations inside the cladding (SCH) regions.

We have developed a comprehensive model for the current noise in semiconductor hetero-junction lasers. The model is self-consistent and includes the carrier density fluctuations in the cladding (SCH) regions. The different processes contributing to the current noise are shown in Fig.4. The noise associated with carrier injection into the active region, carrier recombination and leakage in the cladding regions, carrier capture into and carrier emission from the quantum wells, and radiative and non-radiative carrier recombination in the quantum wells is included in the model. In references [1,2] it is shown that the maximum amount of photon number squeezing achievable in semiconductor lasers is $10\log(1-\eta_o)$ dB, where η_o is the laser output coupling efficiency [9]. We find that the partition noise associated with carrier recombination and leakage in the cladding regions limits the maximum amount of squeezing achievable in semiconductor lasers to $10\log(1-\eta_o\eta_i)$ dB, where η_i is the current injection efficiency defined as the fraction of the total number of carriers injected into the active region that recombine in the quantum wells. This result explains the discrepancy between the maximum amount of squeezing observed experimentally (typically ~ 1-4 dB after correcting for less than unity detection efficiency) and that which is calculated by ignoring the partition noise (typically ~ 7-10 dB) [4]. In reference [3] it was argued that non-zero current injection efficiency would not lead to increased photon noise since coulomb correlations suppress the noise associated with current partitioning in parallel resistive paths. This argument does not hold in charge neutral active regions of semiconductor lasers.

A significant portion of the current noise in semiconductor lasers is a circuit response to the carrier density fluctuations inside the active region. Current noise measurements can therefore provide important information about the high frequency electron-photon dynamics inside the laser. Fig.5 shows the experimental setup for measuring the current noise spectrum of semiconductor lasers at low temperatures. The measurement is made difficult by the low differential impedance of semiconductor lasers, which makes it harder to couple the noise out into the measurement circuit. Fig.6 shows the experimentally measured high frequency current noise spectra as a function of the bias current in an InGaAsP/InP laser operating at 1.55 μm. The current noise spectra show peaks at the laser relaxation oscillation frequency. This is to our knowledge the first observation of relaxation oscillation peaks in the laser current noise. The calculated current noise spectra are shown in Fig.7. Current noise measurements can therefore also be used to study the modulation dynamics of semiconductor lasers completely in the electrical domain without using photodetectors.

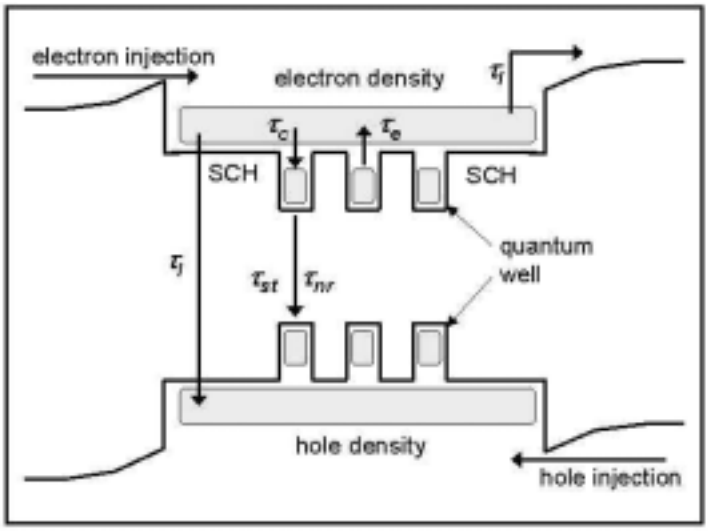

Fig.4 : Energy band diagram of semiconductor quantum well laser showing the various processes contributing to the current noise. The carrier recombination and leakage in the SCH regions also contribute to the current and photon noise.

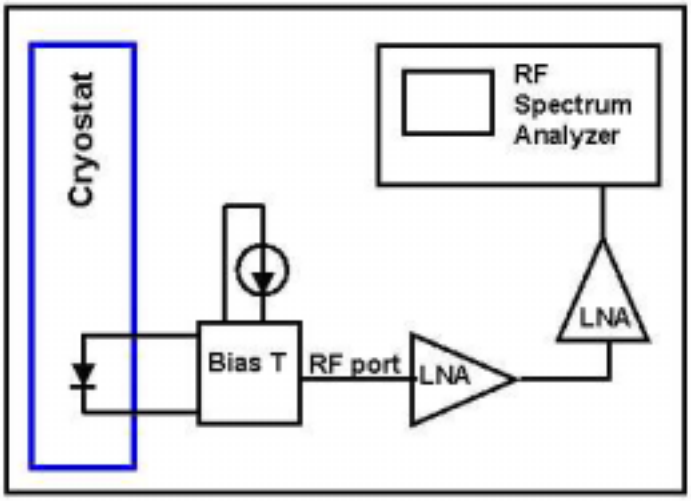

Fig.5 : Low temperature experimental setup for measuring the laser current noise spectrum.

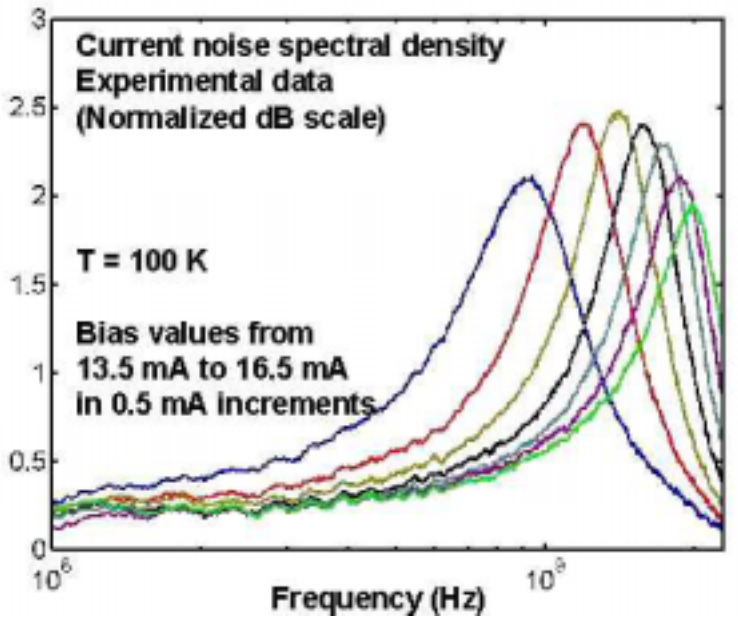

Fig.6 : Spectra (in dB) of current noise measured at different bias currents for a 1.55 μm InP/InGaAsP semiconductor laser. The spectra are normalized to the spectrum a little below threshold (mesurement bandwidth 100MHz – 2GHz).

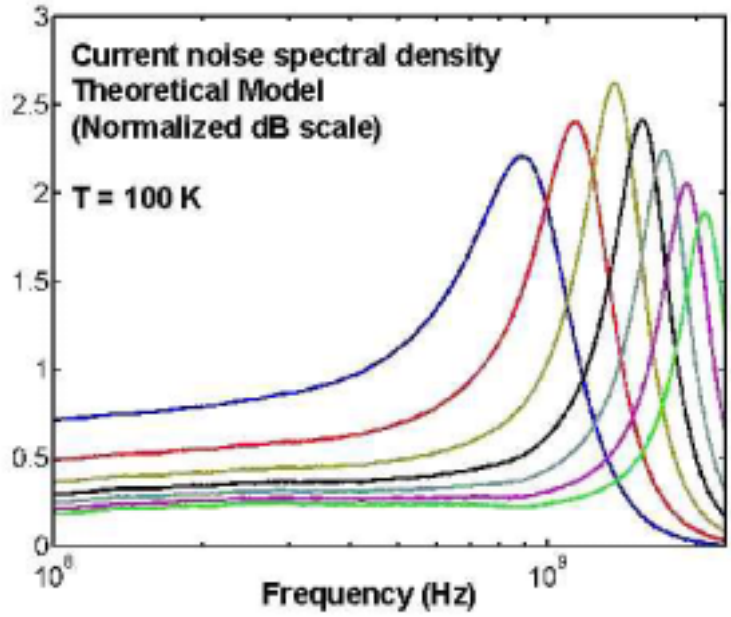

Fig.7 : Calculated spectra (in dB) of current noise for a 1.55 μm InP/InGaAsP semiconductor laser.

References:

1. Y. Yamamoto, N. Imoto, IEEE J. Quantum Electron. **22**, 2032-2042 (1986).
2. Y. Yamamoto, S. Machida, Phys. Rev. A **35**, 5114-5130 (1987).
3. Y. Yamamoto, H. A. Haus, Phys. Rev. A **45**, 6596-6504 (1992).
4. S. Machida, Y. Yamamoto, Optics Lett. **14**, 1045-1047 (1989).
5. G. Bjork, Phy. Rev. A **45**, 8259-8267 (1992).
6. F. Rana, R. Ram, Appl. Phys. Letts. **76**, 1083-1085 (2000).
7. S. G. Patterson, G. S. Petrich, R. J. Ram, L. A. Kolodzjieski, Elec. Letts. **35**, 395-397 (1999).
8. E. Goobar, A. Karlsson, G. Bjork, P-J. Rigole, Phys. Rev. Lett., Jan. 1993, **70**, pp. 437-440.
9. L. A. Coldren, S. Corzine, "Diode Lasers and Photonic Integrated Circuits," John Wiley and Sons, New York (1995).
10. F. Jeremie, C. Chabran, P. Gallion, J. Opt. Soc. Am. B **16**, 460-64 (1999), Appl. Phys. Lett. **75**, 3614-3616 (1999).

Measurement of Correlations in Cascade Lasers

Sponsor

DARPA-RLICS, ONR

Project Staff

Peter Mayer, Farhan Rana, Professor Rajeev J. Ram

Understanding correlations in cascade lasers is important from both a practical and a fundamental perspective. One proposed application of the cascade laser is to improve the slope efficiency of a laser in an optical link. The slope efficiency is an important parameter because the signal-to-noise ratio of an optical link under direct modulation has been shown to scale as the square of the laser slope efficiency. A conventional semiconductor laser emitting photons with perfect quantum efficiency has a slope efficiency of one; for every electron injected into the laser, one photon is emitted from the laser. In a cascade laser, the situation is different because each carrier injected into the laser can sequentially tunnel into each of the multiple active regions, stimulating photon emission in each. Because each carrier injected into an N-stage cascade laser can undergo N photoemission events, the slope efficiency can potentially see an N-fold increase as well. If the noise in each of the photon streams from the N stages is independent of the noise in the other photon streams, the concomitant improvement in the signal-to-noise ratio of the link is expected.

On a more fundamental level, a theory for the photon noise and correlations in semiconductor lasers has recently been developed [1]. Because the gain sections of a cascade laser are electrically connected, carrier density fluctuations and photon emission events in different sections become correlated. The nature of this correlation is sensitive to the configuration of the gain sections (in series as in a cascade laser, or in parallel) and to the impedance of the circuit driving the laser. If two series coupled gain sections are driven with a small (voltage like) external impedance, the theory predicts a positive correlation in the photon noise of the two lasers. The photon noises of two lasers in a parallel circuit configuration driven with a large (current like) external impedance are predicted to have negative correlation. In both situations, the correlations in the output photon streams are expected to arise from the two sources: the thermal noise of the

series parasitic resistance of each laser, and the intrinsic noise of the heterojunction laser. When the external circuit environments for the two circuit configurations are swapped (series coupled lasers driven by a current source, and parallel coupled lasers driven by a voltage source) the correlations between the two beams of light should become small.

This theory has been tested using two single-mode, high output power GaAlAs heterojunction lasers and two large area high efficiency silicon PIN diodes. Before measuring the noise correlations, the noise of a single laser was characterized under various bias conditions. In Fig. 8, the Fano factor of the photon noise in a single current biased laser between 500 kHz and 600 kHz is plotted as a function of DC detector photocurrent. The Fano factor is defined to be the ratio of the measured noise power spectral density of the photon stream to that of photonic shot noise. The large peak in the measured Fano factor was caused by longitudinal mode hopping which was visible on an optical spectrum analyzer. At large biases, stable single-mode operation could be achieved and the laser quieted down, although squeezing (Fano factor < 1) was not observed.

A diagram of the experimental setup is shown in Fig. 9. The two lasers are biased in either the parallel or series configuration through a bias-T using a very quiet (battery) current supply. A switched capacitor determines whether the lasers see a current bias or a voltage bias at the measured frequencies (50 kHz to 1 MHz). The lasers illuminate large area photodiodes, each biased through a large inductors. The photodiodes are tilted from the normal to the laser to eliminate unwanted optical feedback. The fluctuating photocurrent is measured by two home-made low-noise transimpedance amplifiers and the data is sampled on two channels at 25 MHz with a data acquisition board. Considerable effort went into removing all parasitic sources of spurious correlation with careful circuit layout and shielding. The correlation measure used here ranges between –1 (perfectly anticorrelated) to 1 (perfectly correlated), and is given here for the photocurrents. For the series coupled lasers, a correlation of 0.31 was measured for the voltage bias, and a correlation of 0.05 was measured for the measured for the current bias. For the parallel coupled lasers, a correlation of –0.31 was measured for the current bias, and a correlation of -0.07 was measured for the measured for the voltage bias. These results confirmed the basic predictions of the theory outlined above.

[1] F. Rana and R. Ram, Appl. Phys. Lett. **76**, 1083 (2000)

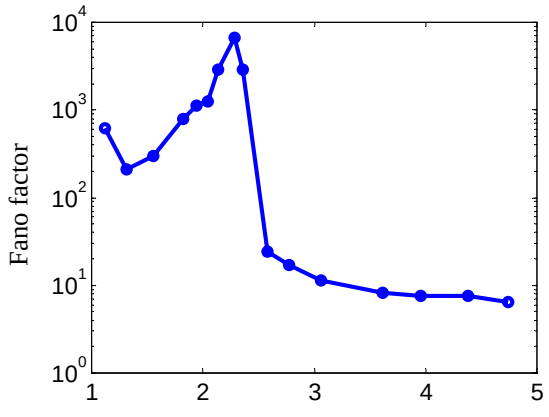

Fig. 8. Measured photon noise Fano factor with vs. laser bias current.

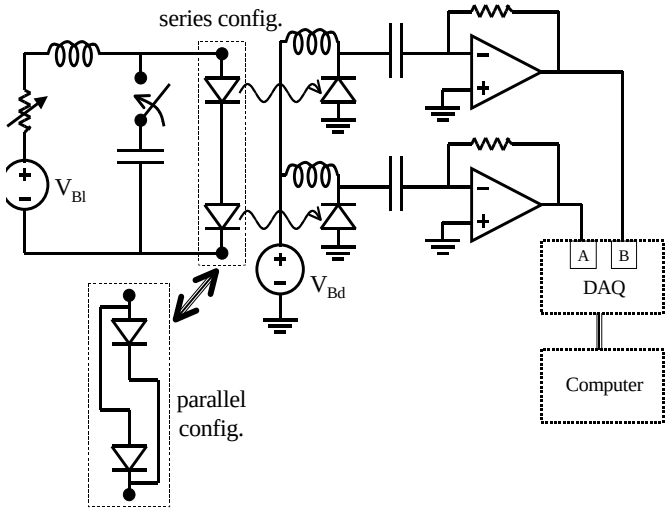

Fig. 9. Experimental setup for the measurement of photon noise correlations. Both the series and the parallel configurations are shown.

Noise in Multimode Surface Emitting Lasers

Sponsor

ONR-MURI

Project Staff

Harry Lee, Professor Rajeev Ram

In previous work, we developed analytic and numerical models for multimode vertical cavity surface emitting lasers. Here, we compare the model results to experiments on a multimode mode oxide aperture VCSEL. Because multimode VCSELs can support partially overlapping multiple transverse modes, their interaction results in low frequency resonance peaks related to the intermode dynamics. Fig. 10 shows a comparison between experiment and radial finite difference VCSEL model, where parts a) and c) show the LI curves and parts b) and d) show the noise spectral density for the individual modes alone and the total noise spectral density. The measured increase in noise at approximately 1GHz is due to the intermode resonance and is captured faithfully in the model, as is the expected anti-correlation between the main and side mode.

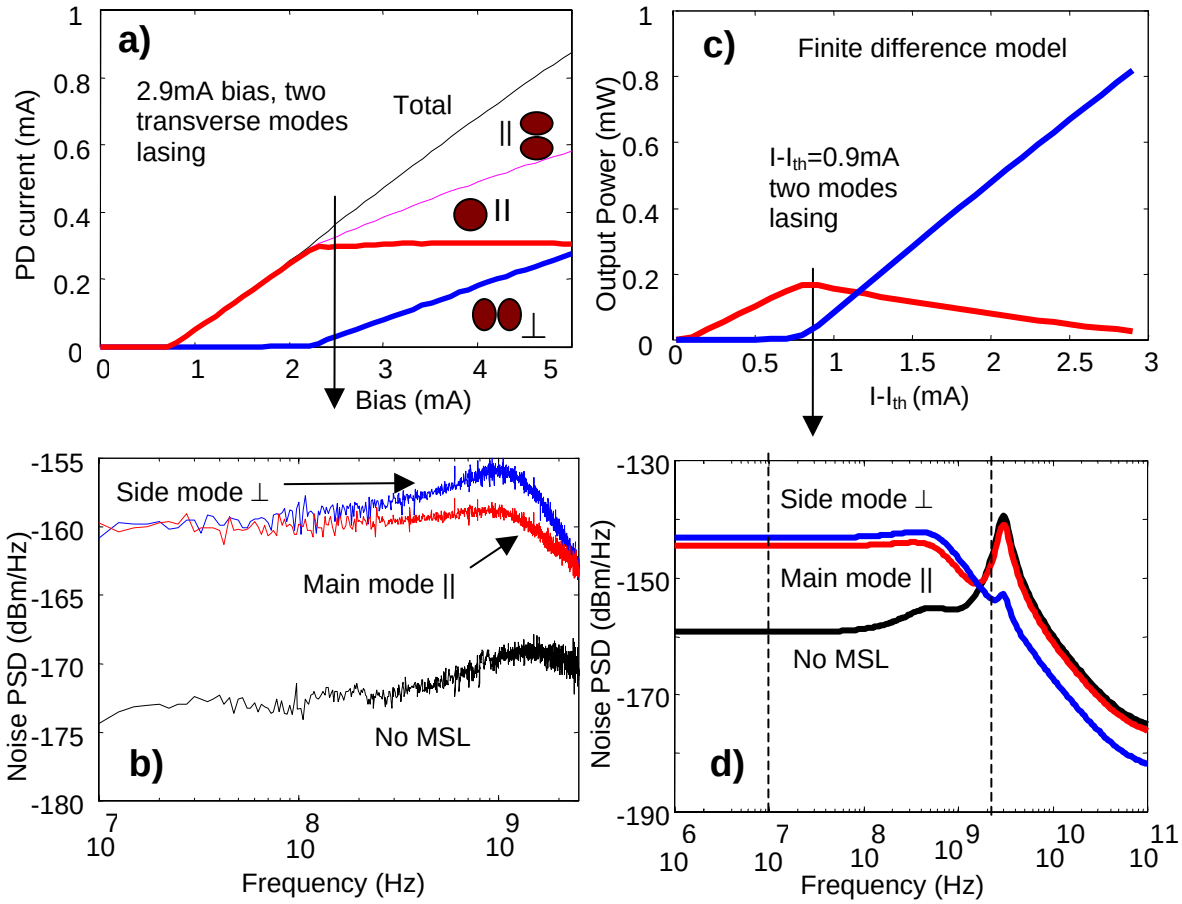

Fig 10. a) Measured polarization resolved LI curve showing transverse mode profile and polarization. b) Noise spectral density for only the main mode, only the side mode, and no mode selective loss. Laser bias = 2.50mA. c) Finite difference LI curve for a two transverse mode model. d) Calculated noise spectral density.

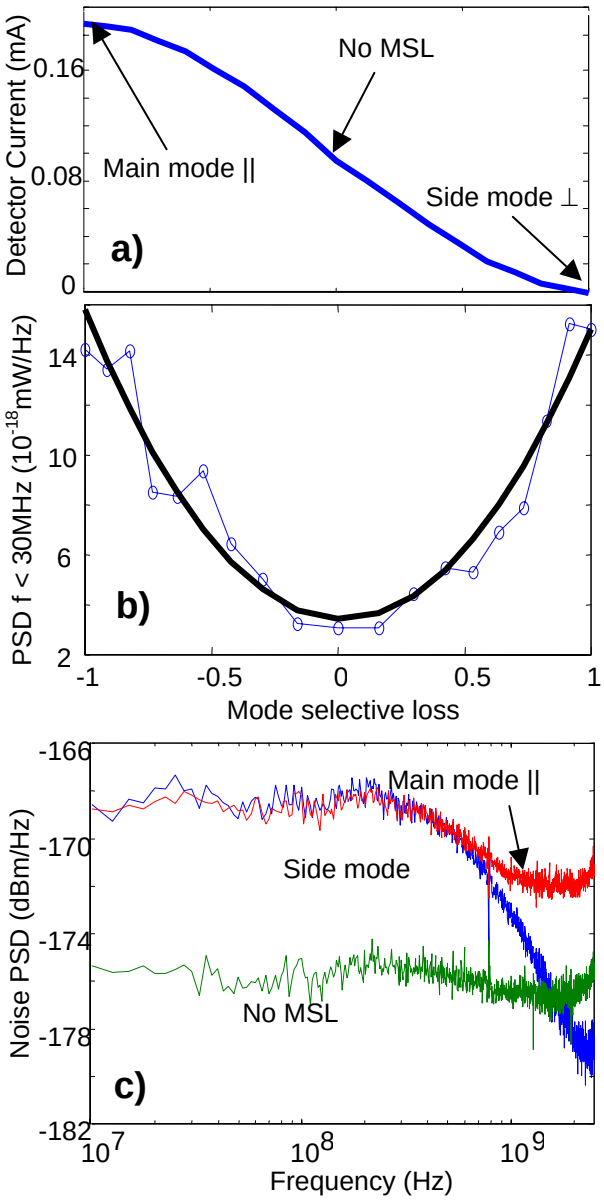

The anti-correlation and dependence of the low frequency noise on the mode selective loss is investigated further in the results of Fig 11. In this experiment, the laser is biased at a point where only a single transverse mode is active with a main and side mode of orthogonal polarization. By rotating a polarizer, the mode selective loss can be adjusted and the noise spectral density vs. mode selective loss was measured. In this case, we observe the interaction of two strongly overlapping modes so the intermode resonance peak disappears. In this situation an analytical solution for the noise is possible and a quadratic dependence on mode selective loss is predicted and verified in Fig 11b). The noise spectral densities in part c) show that the low frequency noise of the main and side modes are equal in magnitude and anti-correlated. The spectral density of the side mode is Lorentzian as expected from the theory.

Fig. 11. a) Photocurrent vs. mode selective loss. b) Corresponding low frequency noise following quadratic dependence. c) Noise spectral density at –1, 0, 1 mode selective loss corresponding to arrows in part a). The VCSEL is biased at 1.50mA where only the fundamental transverse mode is lasing. The side mode is the orthogonally polarized fundamental mode.

Dynamic Range of Surface Emitting Lasers

Sponsor

ONR-MURI

Project Staff

Harry Lee, Professor Rajeev Ram

Our measurements of short free space RF links using multimode VCSELs demonstrated high dynamic range of approximately 100 dB (1Hz bandwidth) at frequencies in the 1-3 GHz range with a maximum measured dynamic range of 110 dB (1Hz bandwidth) at approximately 1GHz. These measurements stimulated some theoretical questions such as, what determines the structure of the dynamic range, and why do multimode VCSELs have performance comparable to edge emitting lasers. Because the transverse mode structure of VCSELs are distinguishing features of these lasers as compared to edge emitting devices, modeling the transverse modes and spatial carrier density inhomogeneity becomes important. To capture these effects, a cylindrically symmetric, radial finite difference rate equation model was developed, including a noise model and a small signal distortion model. Figs. 12 and 13. show the calculated and experimentally measured dynamic range. Model parameters were chosen to fit the DC light-current curve near threshold. The structure of the dynamic range is reliably reproduced by the model, which lends confidence to the further interpretation of its output in computational experiments to isolate the dominant mechanisms responsible for the distortion and noise.

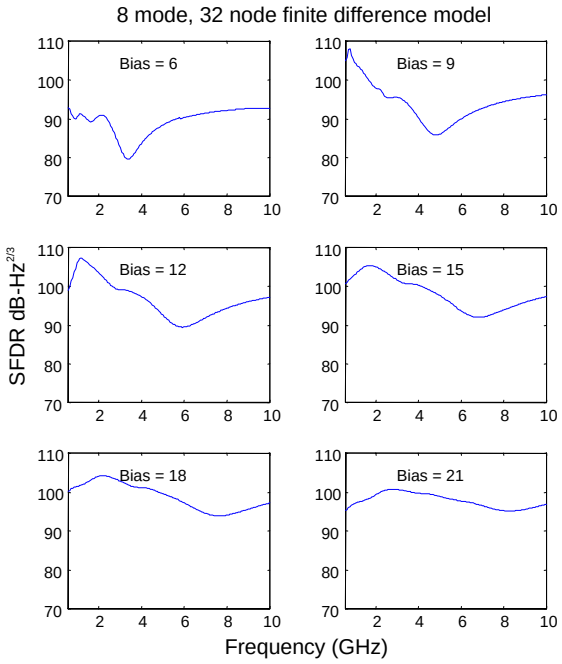

Fig. 2 Simulated dynamic range using 8 mode, 32 node finite difference model.

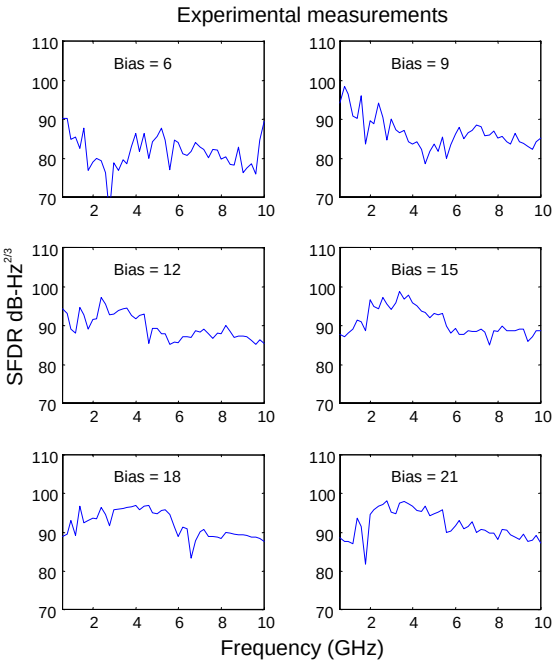

Fig.13 Measured dynamic range vs. frequency for various bias points.

Unidirectional Semiconductor Ring Lasers

Sponsor
Walsin Lihwa Corp.

Project Staff
Song-Ho Cho, Professor Rajeev J. Ram

Photonic integrated circuits (PIC) have the potential to satisfy the trend of telecommunication devices to move toward high capacity [1]. In this context, integrated semiconductor lasers will be associated with various photonic circuits, e.g. optical amplifiers, wavelength converters, transceivers, and routers. However, the necessary optoelectronic integration techniques have not been developed for densely integrated devices, mainly because of the fabrication limitations of cleaved-facet necessity of Fabry-Perot lasers and the vertical optic output coupling of vertical cavity surface emitting lasers.

Since monolithic semiconductor ring lasers do not need cleaved facets, these lasers can be easily integrated with other types of sophisticated microphotonic devices, a step toward large-scale PIC. Due to the definite ring size determined by lithography, unlike Fabry-Perot lasers with cleaved facets, the repetition rate in ring laser operation is well controlled. Furthermore, the ring lasers eliminate spatial hole burning due to traveling wave operation, which results in high side mode suppression ratio and reduced sensitivity to feedback. The high side mode suppression ratio should reduce mode partition noise with a single frequency operation. Also, unidirectional ring lasers can be robust since spurious intracavity reflections can be dumped into the nonlasing direction of propagation within the resonator. Although numerous semiconductor ring lasers have been fabricated, such as squared, triangular, and circular resonators, most of them could not eliminate mode-competition or bistability, because of the bi-directionally propagating lasing modes.

Inherently, ring lasers are bi-directional due to the reciprocity of the gain medium in the ring resonator, so most ring laser systems need a Faraday isolator to obtain unidirectional operation. Unfortunately, monolithically integrable isolators are not available in PIC. In semiconductor circular ring lasers, unidirectional operation has been demonstrated by breaking reciprocity of the ring resonator with a crossover segment [2]. Although unidirectional lasing at a single frequency continuous wave has been demonstrated with an active S crossover waveguide, theoretical analysis has not been developed and the designs have not been extended to single transverse mode waveguides. Another approach to unidirectional operation with a ring resonator introduces a retro-reflecting mirror at the end of one arm of the output to enhance the other output beam, subsequent to the unidirectional operation of a He-Ne ring laser [3]. By incorporating a coupling feedback with a retro-reflector of a distributed Bragg grating or a cleaved facet into the ring resonator, beam propagation tends to be dominant for the one direction.

Following this approach, we carefully design and analyze unidirectional continuous wave circular ring lasers without using an isolator in the beam path that operate a single longitudinal and transverse mode at telecommunication wavelength range toward a new generation of PIC [4]. To enforce the unidirectional and single transverse mode operation, we design a ring laser by cascading scattering matrix whose components are analyzed with finite difference time domain simulation.

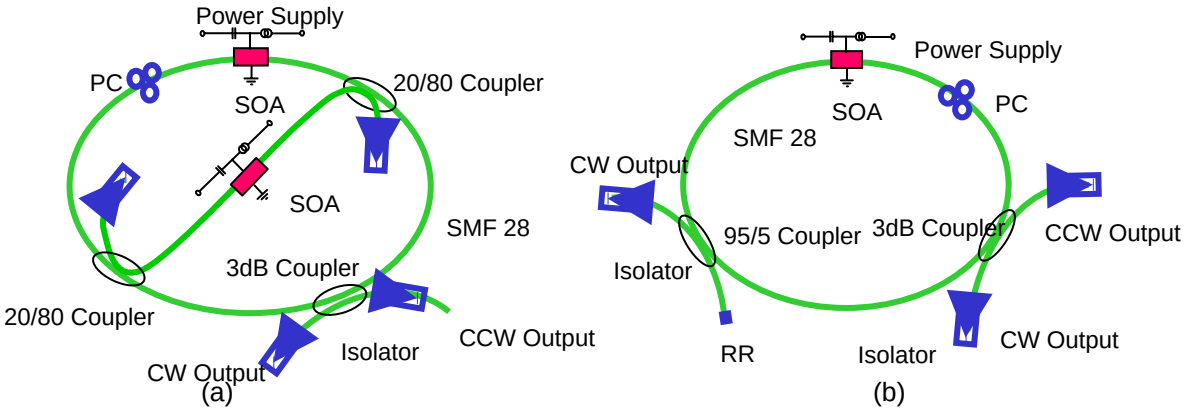

Fig. 14 (a) Unidirectional macroscopic ring laser where S crossover waveguide is incorporated. The laser consists of a semiconductor optical amplifier and single mode fiber. The circulating beam is coupled out with a 3dB fiber coupler and unnecessary beams are blocked with isolators; SMF 28, single mode fiber at 1.55 μm; PC, polarization controller. (b) Unidirectional macroscopic ring laser where a retro-reflector is incorporated; RR, retro-reflector.

As a preliminary approach, hybrid semiconductor fiber ring lasers with a macroscopic S crossover waveguide (Fig.14 a) or a fiber pigtailed retro-reflector (Fig 14. b) are developed to demonstrate unidirectionality. These macroscopic prototype lasers are made with semiconductor optical amplifiers (SOA) as gain media and single mode optical fibers as waveguides. For these lasers, the output power ratio between the two directions of propagation which we refer to as, the counter mode suppression ratio (CMSR), is analyzed.

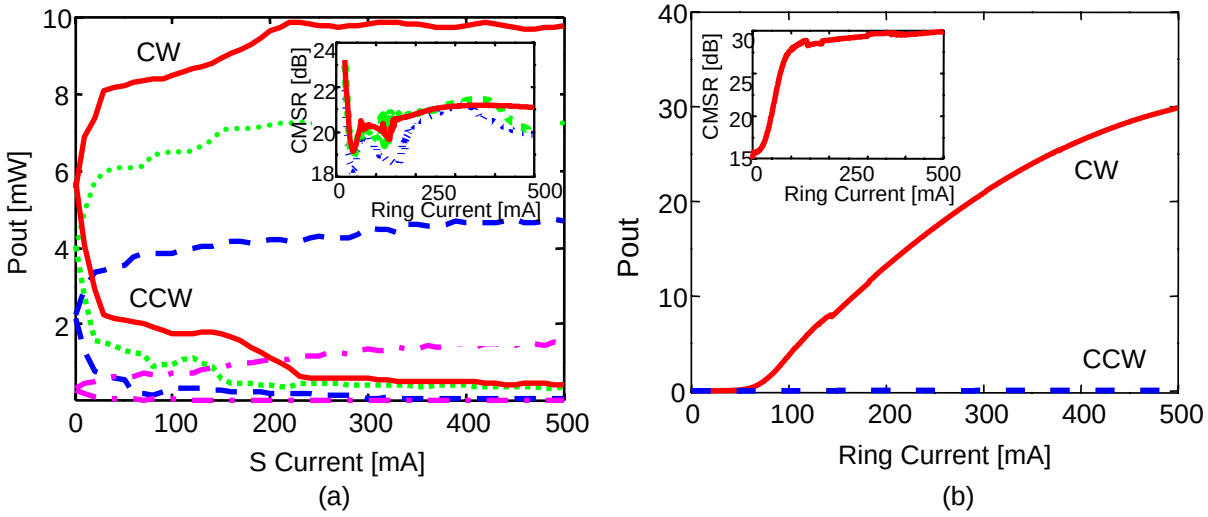

Fig. 15 (a) Counter mode suppression ratio with the fixed S crossover current as the current in the ring increases; solid line, the current to the S crossover segment of 200 mA; dot line, 400 mA; dash line, 300 mA. (b) Counter mode suppression ratio as the current to the ring increases in retro-reflected ring lasers.

For macroscopic S crossover ring lasers, the threshold current of clockwise (CW) and counter-clockwise (CCW) lasing is 33 mA and 36 mA, respectively. Both of spectra are centered at 1590 nm, because the gain is maximal at 1590 nm around the threshold current. The differential quantum efficiency of CW and CCW lasing is 7.7 % and 0.057 %, respectively. Fig. 15(a) shows the unidirectionality of lasing due to spontaneous reciprocity breaking with the fixed ring current as the current to the SOA in the S segment, where upper and lower lines show the CW and CCW output power, respectively. The CMSR is increased from around 19 dB to 21.5 dB as the ring current increases in the inset of Fig. 15(a).

For macroscopic retro-reflected ring lasers, a DBR is replaced with a retro-reflector or a fiber Bragg grating. A 5/95 coupler is chosen to maximize the coupling of CCW beam into CW beam by a retro-reflector. The threshold current of CW and CCW lasing is 36 mA and 60 mA respectively and both of spectra are centered at 1590 nm in Fig. 15(b). The differential quantum efficiency of CW and CCW lasing is 11 % and 0.01 %, respectively. The CMSR is increased from around 16 dB to 30 dB as the ring current increases in the inset of Fig. 15(b).

References

1. C. R. Doerr, C. H. Joyner, L. W. Stulz, and J. Gripp, “Multifrequency laser having integrated amplified output coupler for high-extinction-ratio modulation with single-mode behavior,” IEEE Photon. Tech. Lett. **10**, 1374 (1998).

2. J. P. Hohimer, D. C. Craft, G. R. Hadley, G. A. Vawter, and M. E. Warren, “Unidirectional operation in a semiconductor ring diode laser,” App. Lett. **59**, 3360 (1993).

3. F. R. Foxvog, “Modes of a unidirectional ring laser,” Opt. Lett. **5**, 285 (1980).

4. S. H. Cho and R. J. Ram, “Unidirectional semiconductor ring lasers,” IEEE J. Quant. Electron. (to be submitted).

Low Temperature Scanning Probe Microscopy

Sponsor

National Science Foundation

Project Staff

Mathew Abraham(Harvard), Professor Rajeev J. Ram

A low temperature, high-vacuum scanning probe microscope has been installed. The microscope is operational over the temperature range of 5.5 to 300K, and is capable of scanning tunneling microscopy (STM), atomic force microscopy (AFM) and non-contact AFM. Modifications continue to be made in order to incorporate magnetic scanning probe microscopy in the form of magnetic force microscopy (MFM) and other novel sensors such as scanning josephson junction microscopy (SJM).

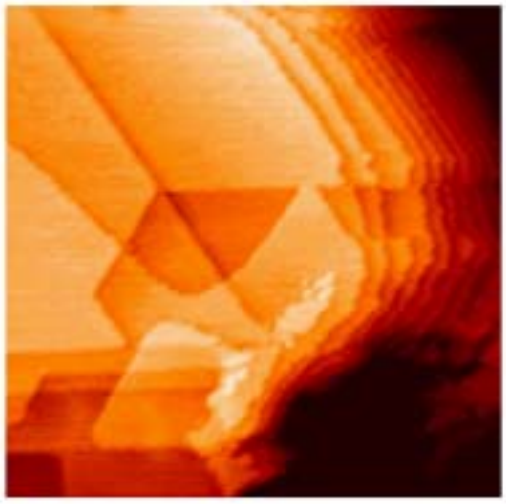

Fig.16 (a). Low temperature, high vacuum scanning probe microscope. Temperature range 5.5K-300K. (b). A 455 x 455 nm^2 STM scan taken at room temperature and high-vacuum showing monoatomic gold steps on a gold sample. Each step is 0.27nm in height.

The magnetic scanning probe microscopy (MFM and SJM) being developed would enable applications such as imaging currents inside mesocopic devices, studying the super-paramagnetic transition of single domain nonomagnetic particles and thin film magnetic storage media.

Fabrication of 2D Electron Gas Devices

Sponsor

National Science Foundation

Project Staff

Mathew Abraham(Harvard), Mark Mondol, Professor Rajeev J. Ram, Professor Henry I. Smith

Mesoscopic quantum effect electronic devices in semiconductor heterostructures have been studied extensively over the past few decades. Most of the experiments have focused on the quantum nature of the electronic wavefunction and have been studied in systems where electron transport is ballistic. More conventional devices in which electron transport is diffusive (or ohmic) have been understood for a long time. Indirect experimental evidence and theoretical calculations imply that the transition between the ballistic and diffusive regimes, in the case of a high mobility two dimensional electron gas (2DEG), involves an intermediate regime that displays "hydrodynamic" like behavior [1].

In semiconductors, the transition from the ballistic to diffusive (ohmic) regime occurs as the electron-phonon scattering length (*lep*) become comparable to the device length. For the most part, the electron-electron scattering length (*lee*) is ignored because the elastic nature of the scattering implies that the classical conductance of a device does not change as *lee* is varied. However, when the electron-electron scattering length is much smaller than the electron-phonon scattering length a hydrodynamic regime for electron transport should occur. Figure 17 shows the electron-electron and electron-phonon scattering length as a function of electron density for various temperatures in a 2DEG GaAs/AlGaAs heterostructure. The shaded region shows the regime where we would expect to see hydrodynamic behavior if the electron temperature and the lattice temperature are both maintained at 10K. The hydrodynamic region could be further enlarged by raising the electron temperature without raising the temperature of the lattice thus maintaining *lep* but reducing *lee*.

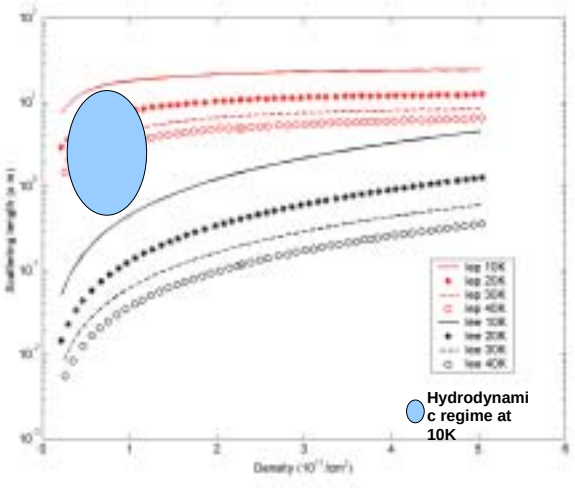

Fig. 17. Electron-electron scattering lengths *lee* and electron-phonon scattering lengths *lep* in a 2DEG GaAs/AlGaAs heterostructure as a function of electron density for temperatures 10K, 20K, 30K and 40K. The shaded region shows the regime where we would expect to see hydrodynamic behavior if the electron temperature and the lattice temperature are both maintained at 10K

The devices that are being fabricated are specifically designed to explore the hydrodynamic regime. These devices are of length scales smaller than *lep* but several times larger than *lee.* Also, it is known that quantum point contacts (QPCs) exhibit quantized conductance and thermopower, and can be used to measure the electronic temperature of a 2DEG [2]. Experiments are being designed incorporating QPCs into devices, so as to be able to

simultaneously measure electron temperature along with the conductance of the device. These devices will probe quantitatively the intermediate regime between ballistic and diffusive transport.

Figure 18 shows gold schottky gates made using e-beam lithography, that define a quantum point contact (QPC) on a 2DEG GaAs/AlGaAs heterostructure substrate.

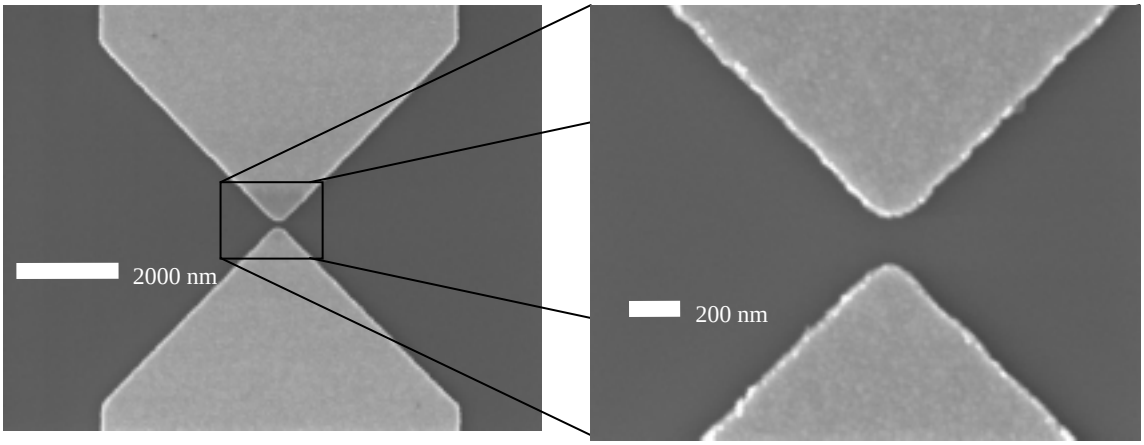

Fig. 18. SEM image of gold schottky gates made using e-beam lithography used define a quantum point contact (QPC) on a two dimensional electron gas (2DEG) GaAs/AlGaAs heterostructure substrate. The QPC exhibits quantized thermopower and can therefore be used to measure the electronic temperature of the 2DEG.

[1] M.J.M. de Jong and L.W. Molenkamp, Phys. Rev. B, **1**,p13389 (1994)
[2] C. W. J. Beenakker and H. van Houten, Solid State Phys. **44**, 1 (1991).

Bipolar Thermoelectric Devices

Sponsor

MIT Lincoln Laboratory, DARPA – University Opto Centers

Project Staff

Kevin Pipe, Professor Rajeev J. Ram, Professor Ali Shakhouri (UCSC)

Thermal management is important for many microelectronic devices due to the performance losses that accompany heat generation, and is often accomplished through the use of an external thermoelectric cooler. Such coolers operate on the principle of the Peltier effect: when carriers move across a junction between two materials in which they transport a different amount of energy, heat is exchanged with the surrounding lattice to make up the difference. In the case of the Peltier cooler shown in Figure 19a, carriers must gain energy as they pass from a metal contact into a semiconductor due to the energy constraint imposed by the semiconductor's density of states. If an array of n-type and p-type blocks are placed electrically in series but thermally in parallel, an applied current will cause a net transfer of heat from one side to the other, cooling one side of the array.

In certain devices it is not desirable to mount an external cooler that can be costly and bulky. An alternative solution is to optimize the thermoelectric behavior of the device itself so that cooling is

achieved internally. For the fundamental case of the diode, as shown in Figure 19b, the thermoelectric description is significantly more complicated than the conventional unipolar cooler due to the diode's bipolar nature.

The Seebeck coefficients for the diode's n-type and p-type regions (related to the average carrier transport energy) have components for both majority and minority carriers, and are also bias-dependent due to the change in carrier concentration with injection [1]. Since the electron and hole quasi-Fermi levels are approximately constant throughout the quasi-neutral regions, average hole and electron Seebeck coefficients can be assigned to each region, as shown in Figure 20. Carrier transport was calaculated by solving the drift-diffusion equations self-consistently with Poisson's equation. The heat exchange at the contacts and junction can be plotted as a function of bias, as can the internal temperature profile. Analytic expressions have been obtained for lightly-doped diodes in the Boltzmann limit, and numerical results have been obtained for heavily-doped diodes in the Fermi-Dirac limit. This analysis has also been performed on heterostructure devices, which place additional constraints on carrier energy due to band offsets.

In the short-base case (in which negligible recombination occurs in the quasi-neutral regions), the diode shifts its non-radiative recombination heat sources to the ohmic contacts, where heat is more readily conducted away from the device. Since thermoelectric cooling always occurs at the diode junction due to the built-in potential, this model is especially useful in optimizing the heat exchange in devices whose performance depends on the junction temperature, such as diode lasers.

[1] Pipe, K. P., R. J. Ram, and A. Shakouri. "Bias-dependent Peltier coefficient in bipolar devices." IMECE 2001 Conference Proceedings (ASME), New York, NY, Nov. 2001.

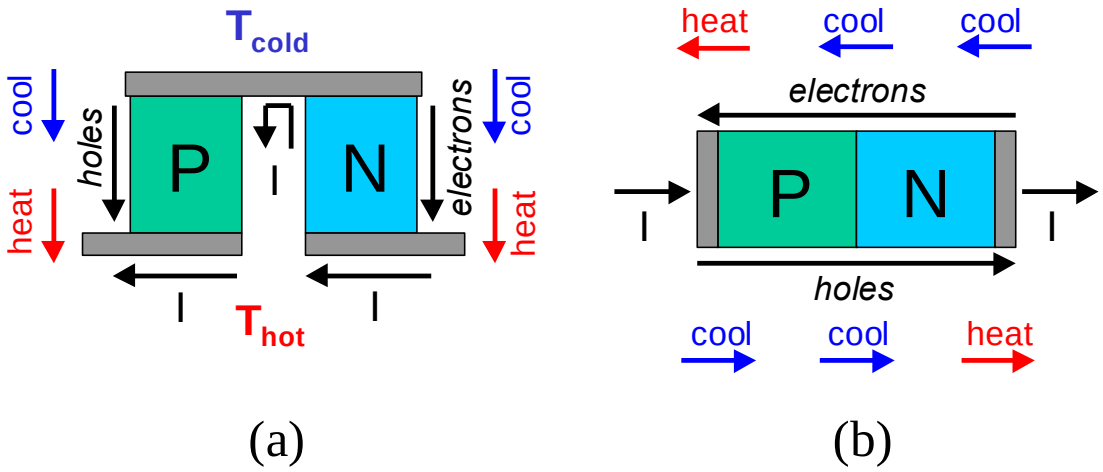

Fig. 19. (a) Conventional Peltier cooler; (b) Diode

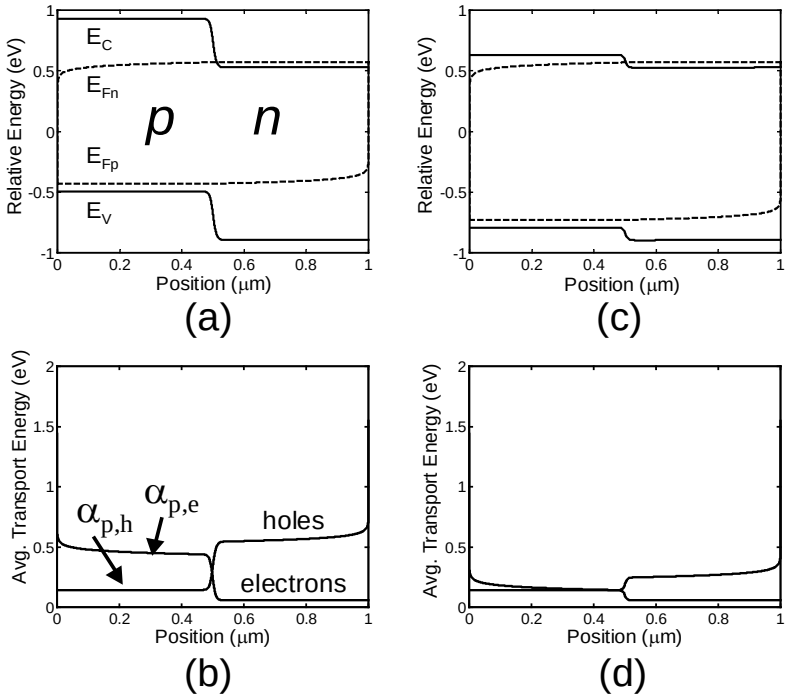

Fig. 20. Homojunction diode: band structure (a,c) and average transport energy (b,d) at 1.00V and 1.30V respectively for a 1 μm GaAs diode doped symetrically at $N_D = N_A = 5x10^{17}$.

Thermal Analysis of Semiconductor Lasers

Sponsor

MIT Lincoln Laboratory, DARPA – University Opto Centers

Project Staff

Kevin Pipe, Professor Rajeev J. Ram, Professor Ali Shakhouri (UCSC)

Heat management can be a critical issue in semiconductor diode laser design due to the strong temperature dependencies of threshold current, quantum efficiency, and device lifetime. In WDM systems, wavelength drift caused by temperature fluctuations can generate crosstalk and intensity noise.

Conventional models for thermal processes in laser diodes only examine the total power dissipated in the device as situated on a thick substrate; effects related to heat flow within the device itself are neglected. These effects have been demonstrated to produce temperature differences of several degrees over micron-thick layers in III-V structures that have been optimized with respect to thermoelectric (Peltier) cooling and thermionic emission [1]. By designing a diode laser so that its bias current produces enhanced thermoelectric cooling within the device itself, temperature stabilization can be achieved without resorting to an (often costly/bulky) external thermoelectric cooler.

The design of such a device relies upon the detailed modeling of internal heat exchange and carrier transport. This has been carried out through the calculation of bipolar Peltier coefficients for each constituent device layer using self-consistent drift-diffusion & Poisson equations. Thermoelectric heat exchange can then be added to terms such as Joule heating and non-radiative recombination in order to derive a heat source distribution; this can then be used to generate a temperature profile for a given laser geometry through the use of finite-element simulation. This model has been used to predict the performance of a novel laser design termed the Injection Current Internally Cooled Light Emitter (ICICLE). The ICICLE structure utilizes Type-II heterointerfaces in order to facilitate thermoelectric cooling of the active region by both injection current into and leakage current out of the core [2]. As shown in Figure 21, the complementary thermoelectric heating terms are shifted to the edges of the devices, where heat is more readily conducted away. These thermoelectric terms can be similar in magnitude to other heat exchange terms in the device (cf. Figure 22); an initial realization of the ICICLE in the GaInAsSb material system has a predicted enhanced cooling of several degrees.

In order to provide experimental verification for the model and for material parameters, correlations have been performed for several conventional 2 μm antimonide lasers between the predicted surface temperature and the temperature as measured by a NIST-calibrated microthermocouple. Further testing will be performed on several GaInAsSb ICICLE structures that have been modeled and subsequently grown at Lincoln Laboratory.

[1] Shakouri, A., C. LaBounty, J. Piprek, P. Abraham, and J. E. Bowers. "Thermionic emission cooling in single barrier heterostructures." Appl. Phys. Lett. **74**, 88 (1999).

[2] Pipe, K. P., R. J. Ram, and A. Shakouri. "Internal thermoelectric heating and cooling in heterostructure diode lasers." Proc. of *Conference on Lasers and Electro-Optics*. Baltimore, MD; May 2001.

[3] Pipe, K. P., R. J. Ram, and A. Shakouri. "Internal cooling in a semiconductor laser diode." Phot. Tech. Lett., to be published in April 2002.

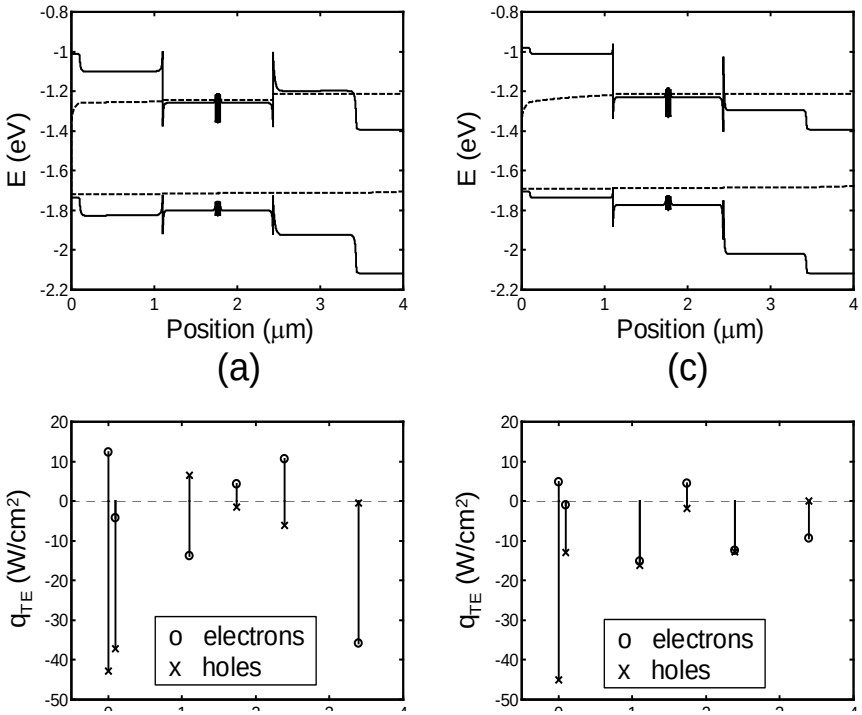

Fig. 21. Band structure and bipolar thermoelectric heat source distribution for GaInAsSb (a & b) conventional separate-confinement heterostructure and (c & d) ICICLE structures at a current density of 475 A/cm^2 [3]. Contact/substrate term is not shown.

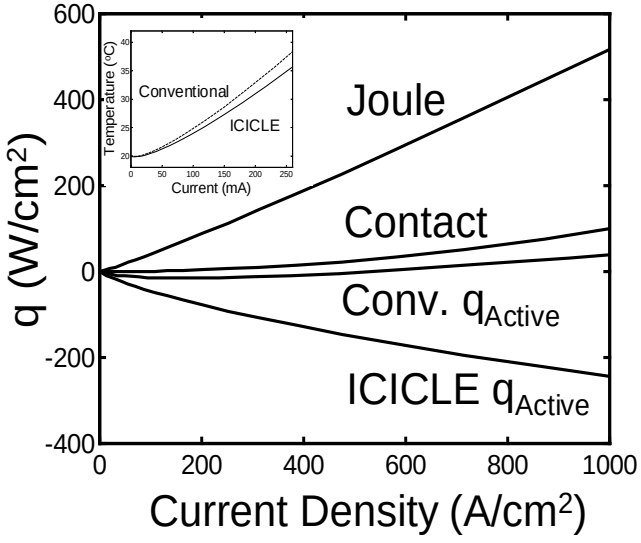

Fig. 22. Heat source terms for GaInAsSb conventional SCH and ICICLE structures. INSET: Calculated quantum well temperature. [3]